Volume 9
Number 12
21 June 2021
Pages 4217-4512

Biomaterials Science

rsc.li/biomaterials-science

Themed issue: Biomaterials Science Emerging Investigators 2021

ISSN 2047-4849

ROYAL SOCIETY OF CHEMISTRY

PAPER

Sidi A. Bencherif *et al.*, *Biomater. Sci.*, 2020, **8**, 7106-7116
Engineering a macroporous fibrin-based sequential interpenetrating polymer network for dermal tissue engineering

European Society for Biomaterials

Biomaterials Science

ROYAL SOCIETY OF CHEMISTRY

PAPER

Cite this: *Biomater. Sci.*, 2020, **8**, 7106

Engineering a macroporous fibrin-based sequential interpenetrating polymer network for dermal tissue engineering†

Olfat Gsib,[a] Loek J. Eggermont,[b] Christophe Egles[a] and Sidi A. Bencherif *[a,b,c,d]

The success of skin tissue engineering for deep wound healing relies predominantly on the design of innovative and effective biomaterials. This study reports the synthesis and characterization of a new type of naturally-derived and macroporous interpenetrating polymer network (IPN) for skin repair. These biomaterials consist of a biologically active fibrous fibrin network polymerized within a mechanically robust and macroporous construct made of polyethylene glycol and biodegradable serum albumin (PEGDM-*co*-SAM). First, mesoporous PEGDM-*co*-SAM hydrogels were synthesized and subjected to cryotreatment to introduce an interconnected macroporous network. Subsequently, fibrin precursors were incorporated within the cryotreated PEG-based network and then allowed to spontaneously polymerize and form a sequential IPN. Rheological measurements indicated that fibrin-based sequential IPN hydrogels exhibited improved and tunable mechanical properties when compared to fibrin hydrogels alone. *In vitro* data showed that human dermal fibroblasts adhere, infiltrate and proliferate within the IPN constructs, and were able to secrete endogenous extracellular matrix proteins, namely collagen I and fibronectin. Furthermore, a preclinical study in mice demonstrated that IPNs were stable over 1-month following subcutaneous implantation, induced a minimal host inflammatory response, and displayed a substantial cellular infiltration and tissue remodeling within the constructs. Collectively, these data suggest that macroporous and mechanically reinforced fibrin-based sequential IPN hydrogels are promising three-dimensional platforms for dermal tissue regeneration.

Received 13th July 2020,
Accepted 10th October 2020

DOI: 10.1039/d0bm01161d

rsc.li/biomaterials-science

Introduction

Over the years, considerable evidence has suggested that various extracellular matrix (ECM) components play a critical role in wound healing.[1–5] Since collagen is the most abundant protein in the dermis layer of the skin, collagen-based scaffolds were among the first artificial ECMs to be developed for dermal tissue regeneration.[6,7] However, their clinical applications have been hindered by several drawbacks such as poor structural integrity and unsatisfactory esthetic outcomes post-implantation.[6,8,9] Other biopolymers including chitosan,[3,10] elastin,[8,9,11] hyaluronic acid[12] and gelatin[1,13] have been investigated for skin scaffold design as well. Yet, these biomaterials did not properly mimic the provisional extracellular matrix formed during the healing process, thereby greatly contributing to irregular scarring after their implantation.[6,8,9,14]

Fibrin, a naturally-occurring biopolymer involved in wound healing, has been widely used in tissue engineering due to its bioactivity, biocompatibility, biodegradability and facile processability.[14] Fibrin-based matrices serve as temporary scaffolds during wound healing in which cells such as fibroblasts adhere, migrate, proliferate and gradually synthesized *de novo* ECM.[14] In addition to its healing properties, fibrin provides the advantage of having its precursors, fibrinogen, and thrombin, easily extractable from blood samples of patients making autologous treatment possible.[14–16] Current fibrin-based biomaterials vary from sheets[17] to sealants[18] and hydrogels.[19–23] Soft, bioactive and tissue-like fibrin-based hydrogels are appealing due to their high water content, making them resemble native soft tissues.[24] Additionally, when fibrin hydrogels are synthesized under physiological conditions, they display biological functionalities similar to those found in the native dermal microenvironment.[14,15]

[a]*Laboratoire de BioMécanique et BioIngénierie (BMBI), UMR CNRS 7388, Sorbonne Universités, Université de Technologie of Compiègne (UTC), Compiègne, France. E-mail: s.bencherif@northeastern.edu*
[b]*Departments of Chemical Engineering and Bioengineering, Northeastern University, Boston, MA, USA*
[c]*Department of Bioengineering, Northeastern University, Boston, MA, USA*
[d]*Harvard John A. Paulson School of Engineering and Applied Sciences, Harvard University, Cambridge, MA, USA*

†Electronic supplementary information (ESI) available. See DOI: 10.1039/d0bm01161d

However, the weak mechanical properties of fibrin hydrogels usually prevent their application in load-bearing situations.[14,25] To overcome this limitation, several strategies have been implemented to improve their physical properties. For instance, increasing the concentration of fibrinogen led to stiffer hydrogels,[26] but resulted in microstructures that were too dense for three-dimensional (3D) cell culture.[27,28] Conjugating fibrinogen with synthetic polymers such as polyethylene glycol (PEGylation) was also tested to enhance the mechanical stability of fibrin hydrogels. However, fibrin-based hydrogels made with PEGylated fibrinogen did not perform as well as those made with unmodified fibrinogen.[29]

Alternatively, interpenetrating polymer networks (IPNs) provide great means to structurally reinforce naturally-derived hydrogels.[1,30–32] An IPN is a construct comprising of at least two polymer networks that are intertwined on the molecular scale without covalent bonds between them.[33,34] Various synthetic routes have been investigated to fabricate IPNs. IPNs are either (i) fabricated with a simultaneous pathway by creating all polymer chains at the same time by independent, non-interfering routes[26,34] or (ii) with a sequential pathway, in which the secondary network is created around the first one, once fully synthesized.[33,35]

IPNs combining fibrin fibers entangled with other biopolymers exhibit reinforced mechanical strengths when compared with each polymer network individually.[30,36,37] Incorporating synthetic polymers such as polyethylene glycol (PEO or PEG)[26] and polyvinyl alcohol (PVA)[28] could further improve their physical properties. While these semi-synthetic IPNs exhibited suitable mechanical and biological characteristics, they did not provide suitable degradable networks.[26,28] Serum albumin (SA), a naturally-derived and degradable protein, has been incorporated into synthetic IPNs to enable enzymatic biodegradation.[38] Yet, these IPNs did not exhibit large and interconnected pores which are of critical importance for tissue engineering applications.[39,40] Ideally, IPNs should display interconnected macroporous architectures to ensure neovascularization,[41] cellular infiltration and organization,[42,43] adequate diffusion of nutrients to cells within the construct as well as *de novo* tissue synthesis and remodeling.[39,40,42,43]

To address these limitations, we recently engineered and characterized a new type of macroporous sequential IPN hydrogels combining the intrinsic biological properties of fibrin with the remarkable mechanical features of PEG. First, methacrylated SA (SAM) was copolymerized with PEG dimethacrylate (PEGDM) to form enzymatically degradable PEGDM-*co*-SAM hydrogels. Next, these hydrogels were subjected to several freeze–thaw cycles (*i.e.*, cryotreatment) to create interconnected macroporous networks. Lastly, cryotreated PEGDM-*co*-SAM hydrogels (1st intertwined network) were swollen into aqueous solutions (water or HEPES buffer) containing fibrin precursors (fibrinogen and thrombin) which were sequentially polymerized to form a 2nd intertwined network, giving rise to sequential IPNs. The physico-chemical properties of IPNs, consisting of cryotreated PEGDM-*co*-SAM networks entangled with fibrin fibers, were thoroughly characterized. Subsequently, their biological properties were assessed using human dermal fibroblasts (HDFs) from neonatal foreskin. Lastly, preliminary *in vivo* studies were performed to assess their biocompatibility, biointegration, and biostability in mice.

Experimental

Materials

Polyethylene glycol (PEG, 4k) (MM = 4000 g mol^{-1}), methacrylic anhydride (MA), diethyl ether, dichloromethane, triethylamine (TEA), ammonium persulfate (APS), *N*,*N*,*N*′,*N*′-tetramethylethylenediamine (TEMED), sodium chloride, calcium chloride, methacrylic acid *N*-hydroxysuccinimide ester (NHSM, purity ~98%), albumin from bovine serum (purity 98%), sodium chloride, propidium iodide, Hoechst 33342, anti-fibronectin antibodies produced in rabbit, acetone were purchased from Sigma-Aldrich. Deuterium oxide and NMR tubes were purchased from Eurisotop. CellTiter 96® AQueous one solution cell proliferation assay (MTS) was obtained from Promega. Penicillin–streptomycin, L-glutamine 1 mM, trypsin–EDTA (0.05%), Click-iT EdU Alexa Fluor 488 imaging kit, calcein AM, goat anti-rabbit IgG secondary antibodies coupled to Alexa Fluor 633 conjugates and goat anti-mouse IgG secondary antibodies coupled to Alexa fluor 488 conjugates were purchased from Life Technologies. Dulbecco's modified eagle medium (DMEM), serum HyClone and six mm biopsy punches were obtained from Dutscher. HDFs from neonatal foreskin were purchased from Cascade Biologics™. Rabbit fluorescein isothiocyanate (FITC)-labelled anti-fibrinogen antibodies were obtained from Dako, North America, Inc. Thrombin from bovine plasma was purchased from Fisher scientific and bovine fibrinogen was obtained from Calbiochem. NHS-rhodamine (5/6-carboxy-tetramethyl-rhodamine succinimidyl ester) mixed isomer was purchased from ThermoFisher. HEPES (4-(2-hydroxyethyl)-1-piperazineethanesulfonic acid, purity 99%) was purchased from Acros Organics. Boric acid and mouse monoclonal, sterile (50 ml) 0.22 μm disposable vacuum filtration system Steriflip® and anti-collagen type I antibodies were purchased from Merck Millipore. Phalloidin fluor 647 reagent was obtained from Abcam. Paraformaldehyde (PFA) 16% solution was purchased from Oxford Instruments. Formaldehyde 4% buffered (pink) Q Path®, saffron alcoholic solution Q Path® and optimal cutting temperature (OCT) compound were obtained from VWR. For animal studies, 5-week old nude mice (NMRI-Foxn1/foxn1nu, male) were purchased from Janvier Labs. Biological implants CELLIS® composed of acellular porcine collagen dermis were obtained from Meccellis Biotech. POLIGLECAPRONE 25 sutures were purchased from Vetsuture®.

Synthesis and characterization of PEGDM

PEGDM was prepared from 4K PEG and MA. PEG (20 g, 0.005 mol), MA (3.86 g, 0.025 mol) and TEA (0.8 mL) were reacted in dichloromethane (60 mL) for 2 days at room temperature. The solution was then precipitated into diethyl ether and the product was subsequently filtered and dried in a vacuum

oven for 5 days at RT. ^{1}H nuclear magnetic resonance (NMR) spectra (270 MHz) were taken on an NMR Avance DSX 400 (Bruker, Germany) to evaluate the degree of functionalization of PEGDM (Fig. S1†). Deuterated oxide (D_2O) was used as a solvent and the polymer concentrations were 2.0% by mass fraction. All spectra were run at RT, 20 Hz sample spinning, 30° tip angle for the observation pulse, and a 10 s recycle delay, for 64 scans.

Synthesis and characterization of SAM

Bovine SA was functionalized with methacrylate residues following a previously published procedure.[15,38] Briefly, 4% w/v bovine SA was solubilized in 0.25 M boric acid buffer at pH 7.4 and then incubated at 37 °C until complete dissolution. Next, NHSM was dissolved in acetone and added dropwise to the SA solution. The reaction took place under stirring overnight at RT. The resulting SAM was then purified by dialysis against 0.01 M HEPES at pH 7.4. Dialysis baths were replaced 3 times (after 2, 6 and 24 h). Next, purified SAM was lyophilized and stored at −80 °C. Before use, SAM was weighed, dissolved in water (200 mg ml^{-1}) and sterile filtered (0.22 μm). A TNBS assay was performed to evaluate the degree of functionalization of SAM (Fig. S2†).

Fabrication of fibrin/PEGDM-*co*-SAM IPN hydrogels

A schematic of the hydrogel formation is presented in Fig. 1. Different formulations of PEGDM-*co*-SAM hydrogels were prepared by mixing PEGDM at various concentrations with SAM in deionized water. The concentrations of (5% w/v) of PEGDM and (5% v/v) of SAM were identified as described by others,[28,38] using similar formulations. Additionally, a higher concentration of PEGDM (15% v/v) was also tested in order to obtain hydrogels with higher stiffnesses.

APS and TEMED (Sigma-Aldrich) solutions were added to the pre-gel solutions at the following concentrations: 0.4% and 1.6% v/v for $PEGDM_5SAM_5$ and 0.1% and 0.4% v/v for $PEGDM_{15}SAM_5$, respectively. Immediately after mixing, the solutions were quickly vortexed and then transferred into Teflon molds. The formed hydrogels were then swollen in deionized water, stored at −20 °C for 2 h and freeze-dried. This cryotreatment process was repeated three times. Next, a total of two fibrin formulations in water (0.5 and 1% w/v) were formed by mixing bovine fibrinogen with thrombin (0.2 U ml^{-1}) in deionized water. These fibrin formulations were referenced as $Fb(0.5\%)_{H_2O}$ and $Fb(1\%)_{H_2O}$, respectively. $Fb(0.5\%)_{HEPES}$ networks were also formed by mixing the fibrin precursors in a HEPES buffer, pH 7.4 (0.01 M HEPES, 0.15 M NaCl, and 0.02 M $CaCl_2$). Next, freeze-dried PEGDM-*co*-SAM constructs were rehydrated with an aqueous solvent containing the fibrin precursors and allowed to sequentially polymerize and form macroporous fibrin/PEGDM-*co*-SAM IPNs.

Evaluation of the microstructure

Environmental scanning electron microscopy (ESEM) (XL 30-ESEM® FEG, Philips, Eindhoven, The Netherlands) was used to image the microstructural features of PEGDM-*co*-SAM and fibrin/PEGDM-*co*-SAM gel samples (Fig. 2). Pore diameters were quantified from the collected ESEM images. Diameters of the longest axes in each of 5 pores per image for a total of 10 images per sample were quantified using Image J software. Confocal laser scanning microscopy (CLSM) (Zeiss LSM 410 invert, Oberkochen, Germany) was used to image the fibrin and PEG networks. PEGDM-*co*-SAM network was labelled with NHS-rhodamine and fibrin was stained with FITC-labelled anti-fibrinogen antibodies.

Swelling ratio measurements

Hydrogels were swollen up to 5 h in phosphate buffered saline (PBS) at 37 °C to reach equilibrium and their weights recorded. The hydrogels were then washed several times in deionized water. The gel samples were subsequently dried, and their weights recorded. The mass swelling ratio (Q_M) was calculated based on eqn (1):

$$Q_M = W_s/W_d \quad (1)$$

where W_s and W_d were swollen gel and dried gel weights, respectively. The swelling data were corrected by subtracting the soluble fraction of salt in PBS from the gel. The swelling ratios measured on fibrin/PEGDM-*co*-SAM IPN hydrogels were then compared to those of cryotreated PEGDM-*co*-SAM hydrogels and to each other (Fig. 3).

Mechanical measurements

Rheological measurements of hydrogels (sample dimensions: 50 mm in diameter and 1 mm in height) were performed using an Anton Paar Physica MCR 301 rheometer with a plate–plate geometry (diameter: 50 mm). We first performed strain and frequency sweeps on PEGDM-*co*-SAM and fibrin hydrogels to select the appropriate strain amplitude (1%) and frequency (1 Hz) (Fig. S3 and S4†). Time sweeps were then performed to determine the gelation point (*i.e.*, the time when storage (G') and loss (G'') moduli crossover) for each formulation and the equilibrium storage moduli (*i.e.*, when G' plateaued) for the different gel formulations either at RT (PEGDM-*co*-SAM) or at 37 °C (fibrin) (Fig. S5†). G' and G'' were next measured on lyophilized PEGDM-*co*-SAM constructs and fibrin/PEGDM-*co*-SAM IPN hydrogels (Fig. 4). The mechanical properties of fibrin/PEGDM-*co*-SAM IPN hydrogels were then compared to those of cryotreated PEGDM-*co*-SAM hydrogels and to each other.

Biological characterization of cell-laden fibrin/PEGDM-*co*-SAM IPN hydrogels

Cell culture. Following the second cryotreatment, PEGDM-*co*-SAM hydrogels were incubated overnight in 70% ethanol, rinsed several times with deionized water and freeze-dried for the third time in a sterile environment. Fibrin precursors were prepared in sterile conditions and filtered using 0.22 μm filters. Next, HDFs were suspended in a 0.5% w/v fibrin precursor solution in HEPES and then incorporated into sterilized and cryotreated PEGDM-*co*-SAM hydrogels. Additionally, HDFs in cell culture medium were seeded on sterilized fibrin/PEGDM-*co*-SAM IPN hydrogels made with either 0.5% or 1% w/v fibrin in water.

Live/dead assay. Cells (10^5 HDFs per construct) were cultured within the constructs and cell viability was evaluated after 2 d (Fig. 5). Live cells were stained with calcein AM (2 μg ml^{-1}) and dead cells with red propidium iodide (5 μg ml^{-1}) for 45 min in the dark at 37 °C. Confocal images were collected and cell viability quantified with ImageJ® software. Cell viability was calculated based on eqn (2):

$$\text{Cell viability}(\%) = \frac{\text{total cell number} - \text{total dead cell number}}{\text{total cell number}} \times 100 \quad (2)$$

Metabolic activity. The metabolic activity was performed using the MTS assay following the manufacturer's instructions. Briefly, at each time point (1, 3 and 7 d), the MTS solution was diluted with the cell culture medium at 1 : 6 ratio and the samples (2×10^4 HDFs per construct) were then incubated for 2 h. The absorbance was measured at 490 nm with a microplate reader and data normalized to the day 1 absorbance (Fig. 5d).

Cell imaging. Hoechst/phalloidin staining was performed on fixed (4% PFA) cell-laden fibrin/PEGDM-*co*-SAM IPN scaffolds (2×10^4 HDFs per construct) at various incubation time points: 1, 3 and 7 d. Briefly, after having stained the PEGDM-*co*-SAM networks with rhodamine, the fibrin networks of the rhodamine-labelled hydrogels were stained with FITC-conjugated anti-fibrinogen antibodies while cells were stained with Hoechst 4432 (2 μg ml^{-1}) and Alexafluor 647 conjugated to phalloidin (1 : 100) for 3 h. The samples were then imaged using a CLSM (Zeiss LSM 410 invert, Oberkochen, Germany). High-resolution image stacks were collected with 50 μm separation between slices (*z*-stacks) (Fig. 6, 7 and Fig. S6†).

Subcutaneous implantations. Fibrin/PEGDM-*co*-SAM scaffolds were subcutaneously implanted in mice to assess their biocompatibility and biointegration. All grafting experiments were performed under an animal protocol approved by the Animal Care and ethics committee of Picardy (national reference number 96, CREMEAP). Before the subcutaneous implantations, mice (n = 6 per group) were divided in three different groups to test the following biomaterials: $Fb(0.5\%)_{HEPES}$/$PEGDM_{15}SAM_5$ (group 1), $Fb(0.5\%)_{HEPES}$/$PEGDM_5SAM_5$ (group 2) and commercially available acellular porcine collagen matrix (group 3).

Mice were first anesthetized with 3.5% isoflurane and then the scaffolds (6 mm in diameter and 1 mm in height) were surgically implanted subcutaneously and sutured on both sides of the dorsal midline. Animals were sacrificed at week 4 following implantation. The scaffolds and the surrounding tissues were explanted and fixed in 4% formalin for 24 h. The biopsy specimens were then dehydrated using graded ethanol 70–96–100%, embedded in paraffin, sectioned at 10 μm, and finally stained with hematoxylin eosin (H&E) or hematoxylin eosin saffron (H&ES) (Fig. 8).

Statistical analysis

All values were expressed as mean ± standard deviation (SD). Statistical significance for the mechanical measurements and swelling ratios were determined using a one-way ANOVA test. The different fibrin/PEGDM-*co*-SAM IPN formulations were compared to cryotreated PEGDM-*co*-SAM hydrogels individually and to each other. Statistical significance for the metabolic activity measurements were determined using Kruskal–Wallis and Dunn's tests. The different IPN formulations were compared to each other at various time points (1, 3 and 7 days). Differences were considered significant at $*p < 0.05$, $**p < 0.01$, and $***p < 0.001$.

Results and discussion

Synthesis of fibrin/PEGDM-*co*-SAM IPN hydrogels

In this work, we aimed to engineer new types of macroporous fibrin/PEGDM-*co*-SAM sequential IPN hydrogels for dermal tissue engineering. IPNs are multicomponent polymeric alloys that combine the unique characteristics of each individual component in an advanced new system.[33] Herein, we combined the intrinsic biological properties of fibrin with the excellent mechanical properties of a PEG in macroporous sequential IPN networks.[44,45] To this end, PEG and SA were first chemically modified to contain methacrylate residues, allowing formation of radically polymerizable PEGDM and SAM, respectively. The degree of methacrylation for each polymer was quantified by ^{1}H NMR and TNBS assays and was found to be approximately 100% for PEGDM and 67% for SAM (Fig. S1 and S2†). Next, PEGDM and SAM were copolymerized at various concentrations *via* a free radical polymerization process (Fig. 1). PEGDM-*co*-SAM hydrogels were subsequently subjected to three consecutive freeze–thaw treatments to introduce interconnected macroporous networks. This process (*i.e.*, cryotreatment), as well as similar techniques such as cryogelation, have been extensively investigated to generate porous biomaterials.[44–55] The resulting cryotreated constructs were then rehydrated with various solutions containing fibrin's precursors (fibrinogen and thrombin) and then allowed to polymerize spontaneously. Three different fibrin's precursor solutions were prepared: one solution containing HEPES buffer, the resulting network made with 0.5% w/v fibrin was defined as $Fb(0.5\%)_{HEPES}$, and two other solutions containing deionized water, defined as $Fb(0.5\%)_{H_2O}$ and $Fb(1\%)_{H_2O}$. This sequential fabrication process resulted in the formation of macroporous fibrin/PEGDM-*co*-SAM IPN hydrogels as shown in Fig. 1.

Physical characterization of fibrin/PEGDM-*co*-SAM IPN hydrogels

Microstructural characterization. The microstructure of PEGDM-*co*-SAM hydrogels was imaged pre- and post-cryotreatment and following the sequential polymerization of fibrin within the constructs (Fig. 2). The surface of the $PEGDM_5SAM_5$ (Fig. 2a) and $PEGDM_{15}SAM_5$ (Fig. 2b) hydrogels was homogenous with a quasi non-porous (*i.e.*, mesoporous) structure prior to cryotreatment. However, following cryotreatment, the two PEG-based hydrogels exhibited a heterogeneous macropor-

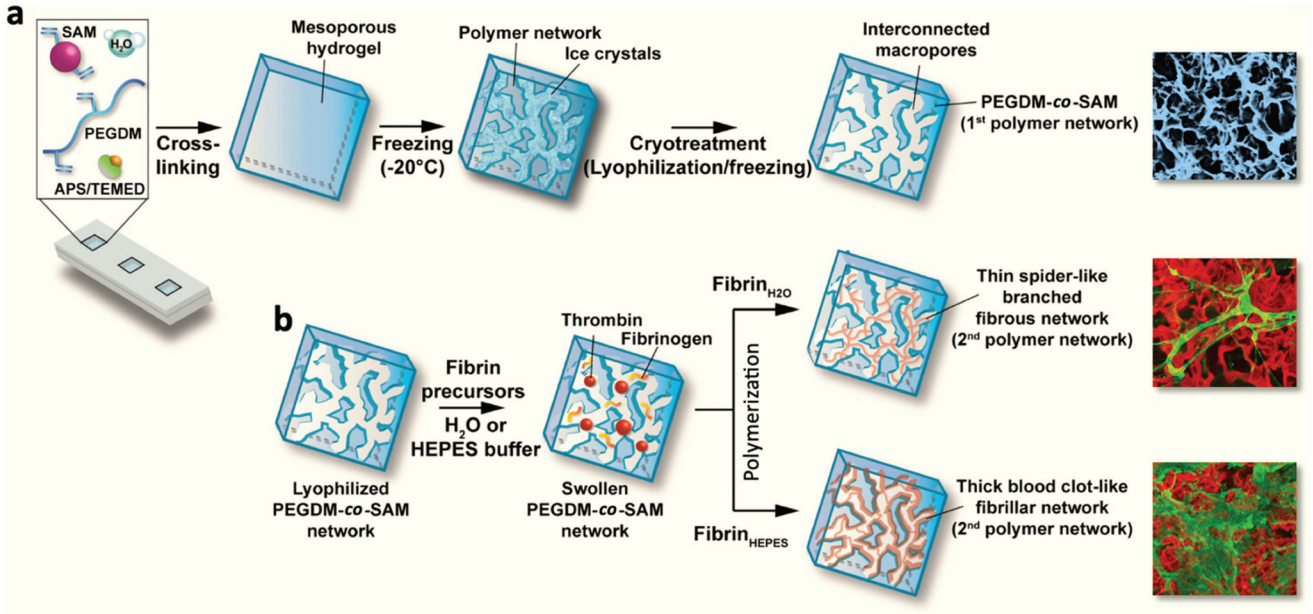

Fig. 1 Schematic depicting the fabrication process of macroporous fibrin/PEGDM-*co*-SAM sequential IPNs. (a) Fabrication of the first crosslinked PEGDM-*co*-SAM network. PEGDM and SAM at various concentrations were copolymerized in water using an APS/TEMED initiator system to fabricate mesoporous PEGDM-*co*-SAM hydrogels. PEGDM-*co*-SAM hydrogels were subsequently frozen at −20 °C and subjected to cryotreatment (*i.e.*, 3 freeze–thaw cycles) to create an interconnected macroporous structure. Pseudocolored (blue) SEM image (right) depicting the macroporous architecture of a cryotreated PEGDM-*co*-SAM hydrogel. (b) Sequential polymerization of the second fibrin network. Cryotreated and lyophilized PEGDM-*co*-SAM scaffolds were swollen with aqueous solvents (HEPES buffer or water) containing fibrin precursors (fibrinogen and thrombin) and polymerized under physiological conditions to form sequential IPNs. Confocal images (right) depicting fibrin (green) and PEGDM-*co*-SAM (red) sequential IPNs.

ous network with mean pore sizes of 74.7 ± 63.8 μm and 65.6 ± 40.1 μm for $PEGDM_5SAM_5$ and $PEGDM_{15}SAM_5$, respectively (Fig. 2a and b). Thus, the PEGDM-*co*-SAM hydrogels displayed a large pore size distribution within the range of 50–200 μm as reported in literature for other scaffolds in skin tissue engineering.[3,10,56–59] Following polymerization within the cryotreated PEG-based hydrogels, fibrin formed a thick blood clot-like fibrillar network when polymerized in HEPES buffer as opposed to a thin and spider-like fibrous network when fabricated in water (Fig. 2a and b).

The fibrous nature of fibrin networks synthesized in water was most likely a result of the precipitation of fibrin in a non-buffered aqueous solution. These data are particularly promising since the dermis is known to have a fibrous cellular microenvironment.[60] The repartition of the two entangled networks, rhodamine-labelled PEGDM-*co*-SAM (in red) and FITC-labelled fibrin (in green), was then imaged by confocal imaging (Fig. 2c and d). Independently of its concentration, a thin fibrous network of fibrin could be observed through the pores when formulated in water (Fig. 2c and d).

Importantly, regardless of the aqueous solvent or polymer composition used, the various fibrin/PEGDM-*co*-SAM IPNs fabricated retained the advantageous macroporous structure of the initial cryotreated PEGDM-*co*-SAM hydrogels. Indeed, sequential polymerization of fibrin did not significantly impact the overall pore size of IPNs which is an essential aspect of tissue engineering scaffolds. This is particularly important for dermal tissue repair, since this process requires sufficient space for cellular colonization and blood vessel formation.[56–59,61]

Swelling measurements. Since hydrogels are defined as three-dimensional crosslinked polymeric networks absorbing large amounts of water,[60] it was crucial to then measure the swelling ratio (Q_M) at equilibrium, which represents the water absorption capacity of hydrogels in their fully swollen state. Q_M was measured before and after addition of fibrin for both cryotreated PEGDM-*co*-SAM formulations (Fig. 3). The swelling behaviour of pure fibrin hydrogels (control) was first evaluated (Fig. 3a). Independently of the polymer concentration, Q_M was significantly higher for fibrin hydrogels fabricated in HEPES buffer than those formed in water. Q_M was approximately 44 *vs.* 8.7 and 9.8 for 0.5% w/v fibrin in HEPES buffer *vs.* 0.5% and 1% w/v fibrin in water, respectively (Fig. 3a). Next, Q_M was also measured for the two cryotreated PEGDM-*co*-SAM formulations (Fig. 3b and c) before and after incorporating fibrin. The addition of the $Fb(0.5\%)_{HEPES}$ to cryotreated PEGDM-*co*-SAM hydrogels increased their swelling ratios. For the $PEGDM_5SAM_5$ formulations, Q_M was approximately 11.8 for fibrin-free cryotreated $PEGDM_5SAM_5$ *vs.* 15.2, 12.7 and 13.1 for fibrin/$PEGDM_5SAM_5$ IPN hydrogels when fibrin was formulated in HEPES buffer (0.5% w/v) and in water (0.5% and 1% w/v), respectively (Fig. 3b).

For $PEGDM_{15}SAM_5$ hydrogels, Q_M was approximately 8 for fibrin-free cryotreated $PEGDM_{15}SAM_5$ *vs.* 9.7, 8.4 and 8.7 for

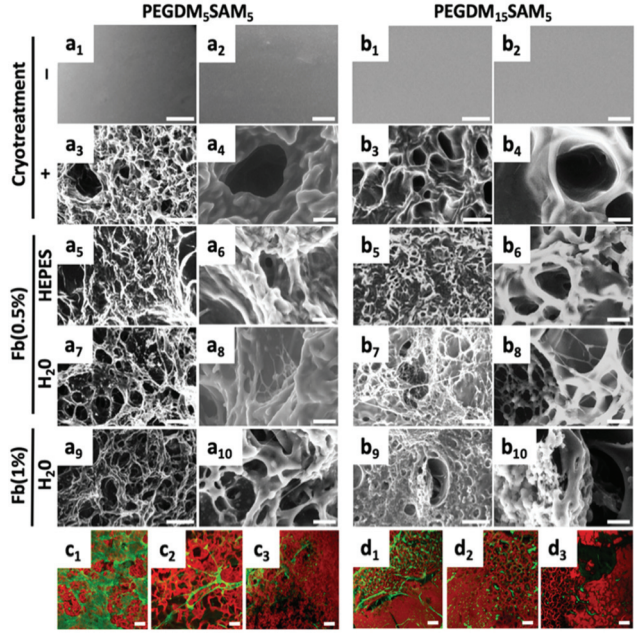

Fig. 2 ESEM and confocal images of pre- and post-cryotreated PEGDM-*co*-SAM and fibrin/PEGDM-*co*-SAM sequential IPN hydrogels. $PEGDM_5SAM_5$ (a) and $PEGDM_{15}SAM_5$ (b) hydrogels were imaged with ESEM pre- (a_1, a_2, b_1, b_2) and post- (a_3, a_4, b_3, b_4) cryotreatment. fibrin/PEGDM-*co*-SAM sequential IPN hydrogels were also imaged across the three investigated fibrin formulations: $Fb(0.5\%)_{HEPES}$ (a_5, a_6, b_5, b_6), $Fb(0.5\%)_{H_2O}$ (a_7, a_8, b_7, b_8) and $Fb(1\%)_{H_2O}$ (a_9, a_{10}, b_9, b_{10}). Scale bars = 100 μm (1, 3, 5, 7, 9) and 20 μm (2, 4, 6, 8 and 10). a_2, a_4, a_6, a_8, a_{10} and b_2, b_4, b_6, b_8, b_{10} are zoomed-in views of images a_1, a_3, a_5, a_7, a_9 and b_1, b_3, b_5, b_7, b_9, respectively. *Z*-Stack confocal images of $PEGDM_5SAM_5$ (c) or $PEGDM_{15}SAM_5$ (d) network stained in red with rhodamine-labelled SAM. The sequential fibrin network was labelled in green with FITC-labelled anti-fibrinogen antibodies for each formulation investigated: $Fb(0.5\%)_{HEPES}$ (1) (c_1 and d_1), $Fb(0.5\%)_{H_2O}$ (c_2 and d_2), and $Fb(1\%)_{H_2O}$ (c_3 and d_3). Scale bars = 100 μm (c and d).

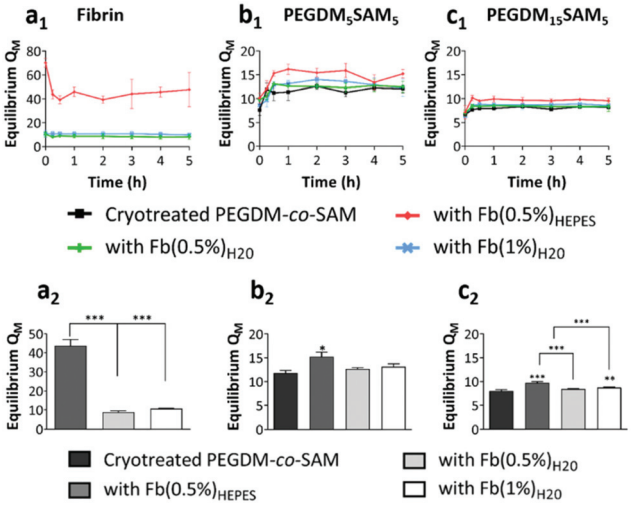

Fig. 3 Swelling characteristics of the various (a) fibrin formulations and (b and c) cryotreated PEGDM-*co*-SAM: swelling kinetics for (a_1) fibrin hydrogels and across fibrin-free and fibrin-containing PEGDM-*co*-SAM hydrogels: (b_1) $PEGDM_5SAM_5$ and (c_1) $PEGDM_{15}SAM_5$. Swelling mass ratio (Q_M) at equilibrium for (a_2) fibrin hydrogels and across fibrin-free and fibrin-containing PEGDM-*co*-SAM hydrogels: (b_2) $PEGDM_5SAM_5$ and (c_2) $PEGDM_{15}SAM_5$. The swelling ratios Q_M at equilibrium measured on the different fibrin-containing PEGDM-*co*-SAM hydrogels were compared to those of fibrin-free cryotreated PEGDM-*co*-SAM hydrogels and to each other. Values represent mean ± SD ($n \geq 3$). Data were analyzed using one-way ANOVA test. *$p < 0.05$, **$p < 0.01$, and ***$p < 0.001$.

fibrin/$PEGDM_{15}SAM_5$ IPN hydrogels when fibrin was formulated in HEPES buffer (0.5% w/v) or in water (0.5% and 1% w/v), respectively (Fig. 3c). The highest swelling ratio observed for IPNs with fibrin made in HEPES buffer could be attributed to a more homogeneous polymerization of fibrin leading to a uniform network when synthesized in a buffered solution, enabling the constructs to absorb and contain more water. It is worth noting that Q_M for fibrin-free cryotreated $PEGDM_{15}SAM_5$ hydrogels was lower than those fabricated with $PEGDM_5SAM_5$ (Fig. 3b and c) showing that increasing the PEG concentration resulted in a decrease in gel swelling. Nevertheless, although the swelling ratio of hydrogels is mainly dictated by the polymer concentration (*i.e.*, crosslinking density), IPN hydrogels tested showed an ability to uptake and retain large amounts of water across the different formulations tested.[60] Overall, the swelling ratios measured for the different IPN hydrogels were in the range of those reported in literature, particularly for gels formulated with equivalent concentrations of SA[62] or PEG.[26]

Evaluation of mechanical properties. Our strategy to reinforce brittle fibrin hydrogels was based on a sequential IPN system in which fibrin was polymerized within a robust and macroporous PEG-based construct. In fact, several studies have already documented that IPN formation is a viable strategy to reinforce the physical properties of mechanically weak polymeric systems.[26,28,30,36] In our study, we performed rheological measurements to ascertain the mechanical stability of our IPNs. We were also able to measure with this technique the impact of the degree of crosslinking on the stiffness of the hydrogels and to identify their gelation point.[63] We first determined the optimal strain (1%) and frequency (1 Hz) to apply for sample characterization (Fig. S3 and S4†) and then, we performed time sweeps to determine the gelation points (Fig. S4†). Next, we measured the storage moduli (G') of the different IPNs and pure fibrin hydrogels (Fig. 4†). The storage modulus of pure fibrin hydrogels (control) was noticeably higher when formulated in HEPES buffer compared to networks made in water, with a G' of 0.2 kPa for $Fb(0.5\%)_{HEPES}$ *vs.* 0.01 and 0.02 kPa for $Fb(0.5\%)_{H2O}$ and $Fb(1\%)_{H2O}$, respectively (Fig. 4a). The superior mechanical strength of fibrin hydrogels made in HEPES buffer is most likely due to the presence of salts and adequate pH (*i.e.*, buffer solution) leading to a thick and mechanically stable clot-like fibrillar network.[64] Several studies have reported the influence of the buffer solution[64] or ion concentrations (*e.g.*, sodium, chloride),[65] on the structure and thickness of fibrin fibers, and ultimately on their physical properties.[66,67] Mechanistically, the poor self-assembly of fibrin in water into a thin and heterogenous spider-like branched fibrous network could explain their poor mechanical performance.

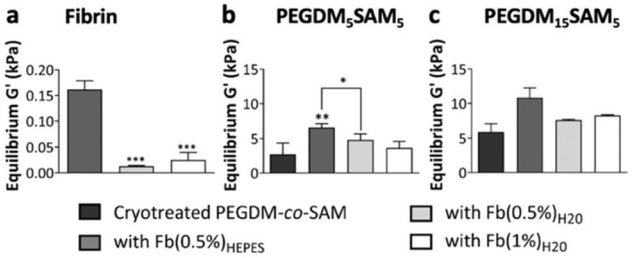

Fig. 4 Elastic moduli at equilibrium for across the various (a) fibrin formulations and for (b and c) cryotreated PEGDM-*co*-SAM: (b) $PEGDM_5SAM_5$ and (c) $PEGDM_{15}SAM_5$ and their corresponding fibrin/PEGDM-*co*-SAM sequential IPN hydrogels when cryotreated PEGDM-*co*-SAM were sequentially polymerized with fibrin. The elastic moduli G' at equilibrium for the different fibrin/PEGDM-*co*-SAM sequential IPN hydrogels were compared to those of cryotreated PEGDM-*co*-SAM hydrogels and to each other. Values represent mean ± SD ($n \geq 3$). Data were analyzed using one-way ANOVA test. *$p < 0.05$, **$p < 0.01$, and ***$p < 0.001$.

Overall, across all the formulations tested, fibrin hydrogels exhibited weak mechanical properties as previously reported by others,[26,28,38] highlighting the importance of engineering fibrin-based hydrogels that are mechanically more stable. We then evaluated the rheological properties of cryotreated PEGDM-*co*-SAM hydrogels, pre- and post-sequential fibrin fabrication (Fig. 4b and c). Our results confirmed that polymerizing fibrin within cryotreated PEGDM-*co*-SAM hydrogels significantly increased their elastic moduli (Fig. 4b and c). The G' was 5.9 kPa for cryotreated $PEGDM_{15}SAM_5$ *vs.* 10.9, 7.8 and 8.2 kPa for fibrin/$PEGDM_{15}SAM_5$ IPNs made with $Fb(0.5\%)_{HEPES}$, $Fb(0.5\%)_{H_2O}$ and $Fb(1\%)_{H_2O}$, respectively (Fig. 4b). Similarly, the G' was 2.7 kPa for cryotreated $PEGDM_5SAM_5$ *vs.* 6.5, 3.7 and 4.8 kPa for fibrin/$PEGDM_5SAM_5$ IPNs made with $Fb(0.5\%)_{HEPES}$, $Fb(0.5\%)_{H_2O}$ and $Fb(1\%)_{H_2O}$, respectively (Fig. 4c). Similarly to previous reports,[28,30,35,37] the mechanical performance of fibrin/PEGDM-*co*-SAM IPN hydrogels was enhanced, most likely due to a contribution of both fibrin made in HEPES buffer and the excellent mechanical properties of the PEGDM-*co*-SAM network itself. Furthermore, as expected and independently of the fibrin formulation tested, the mechanical performance of the $PEGDM_{15}SAM_5$-based hydrogels outperformed those made with $PEGDM_5SAM_5$ (Fig. 4b and c). It is also worth noting that, although cryotreatment may compromise the mechanical integrity of polymeric scaffolds,[42] cryotreated PEGDM-*co*-SAM hydrogels retained sufficient mechanical strength to markedly reinforce the fibrin networks for both PEG concentrations tested.

Overall, our data suggested that fibrin-containing IPN hydrogels exhibited much better mechanical integrity ($G' > 3$ kPa)[26,28,38] than fibrin hydrogels alone (around 0.1 kPa).[28,38] The elastic moduli of the macroporous fibrin/PEGDM-*co*-SAM sequential IPNs were in the range of 0.43–6.6 kPa, which were similar to the mechanical strengths reported for native dermis tissue.[68] Furthermore, the superior mechanical characteristics of our engineered IPN hydrogels surpass what others have previously described. For instance, several studies have already reported fibrin-based IPNs combining a fibrin network intertwined with another naturally-derived polymer network such as alginate[36] or hyaluronic acid.[30,32] However, their elastic moduli did not exceed 0.6 kPa.[32] Additionally, other biosynthetic fibrin-based IPNs combining a fibrin network intertwined with a synthetic polymer such as polyvinyl alcohol (PVA)[15,16,28,38] or PEG[15,16,26] network have also been reported. These fibrin-based materials made *via* photopolymerization were described to be biocompatible, non-retractable and self-supported.[26,28,38] However, their mesoporous network was not compatible with 3D cell culture.[15,16,38] Furthermore, UV-exposure during the photopolymerization process could be harmful to mammalian cells.

Biological characterization of fibrin/PEGDM-*co*-SAM IPN hydrogels

The biomaterials were tested both *in vitro* and *in vivo* to assess their biocompatibility, cellular infiltration, and biodegradation.

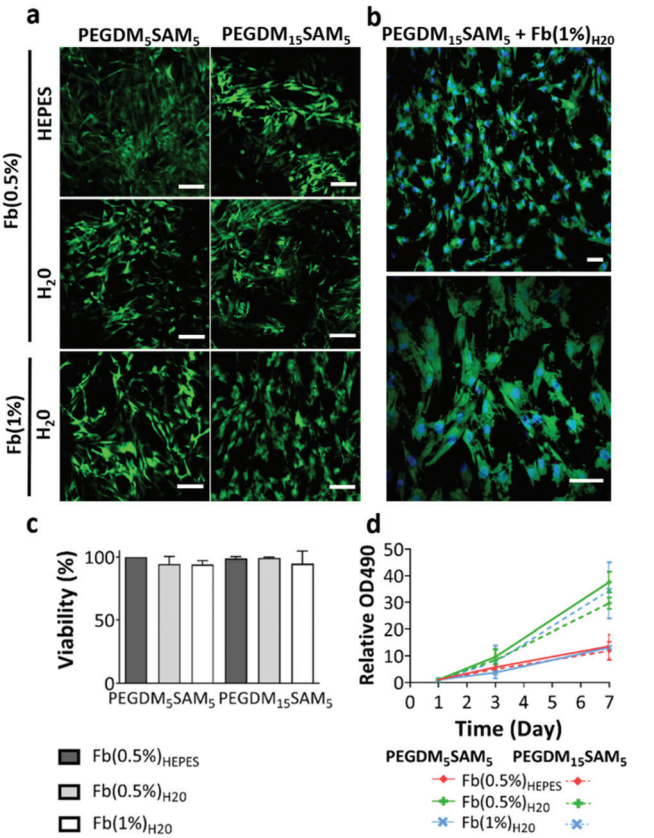

Fig. 5 Evaluation of cell viability and metabolic activity of HDFs in fibrin/PEGDM-*co*-SAM sequential IPN hydrogels: (a) merged confocal microscopy images of HDFs cultured in IPNs after 2 d depicting live (green) and dead (red) cells. (b) Zoomed in images of HDF-laden IPN hydrogels made with $Fb(1\%)_{H_2O}$ showing cell nuclei (blue), live (green) and dead (red) cells. Scale bars = 100 μm (a) and 50 μm (b). (c) Cell viability (%) across fibrin/PEGDM-*co*-SAM sequential IPN hydrogels: fibrin/$PEGDM_5SAM_5$ (left) and fibrin/$PEGDM_{15}SAM_5$ (right). (d) Metabolic activity of HDFs in IPN hydrogels after 1, 3 and 7 d of culture. (c and d) Values represent mean ± SD ($n \geq 3$).

Cytocompatibility and ECM deposition studies. We evaluated the cytocompatibility of engineered IPNs with HDFs from neonatal foreskin. First, cells were seeded into the constructs and their viability evaluated after 2 days of incubation (Fig. 5a–c). Across the different fibrin/$PEGDM_{15}SAM_5$ and fibrin/$PEGDM_5SAM_5$ formulations tested, cell viability remained high (>90%) suggesting their excellent cytocompatibility (Fig. 5a–c). We then examined the metabolic activity of HDFs after 1, 3 and 7 days of incubation (Fig. 5d). The metabolic activity for the different cell-laden constructs was up to 38-fold higher at day 7 when compared to day 1. In particular, metabolic activity increased substantially from day 3 to day 7 suggesting that cells were actively proliferating (Fig. 5d). No statistical differences were found at any point in time between groups with different IPN formulations.

Next, we explored the morphology of HDFs when cultured in the constructs (Fig. 6 and S6†). For each formulation, most fibroblasts adopted their typical spindle-like shape, adhered to the fibrin network and infiltrated the scaffold through their interconnected macropores (Fig. 6 and S6†). These results suggest that the intrinsic properties of fibrin were retained across all the formulations tested and that the macroporous structures of the different hydrogels were favorable for dermal fibroblast culture. Lastly, we investigated whether the scaffolds would promote deposition of collagen I and fibronectin (Fig. 7), two main dermis extracellular matrix (ECM) proteins involved in cell adhesion and protein regulation during wound healing.[69,70] Within one week of culture, HDFs were able to secrete and deposit these two proteins

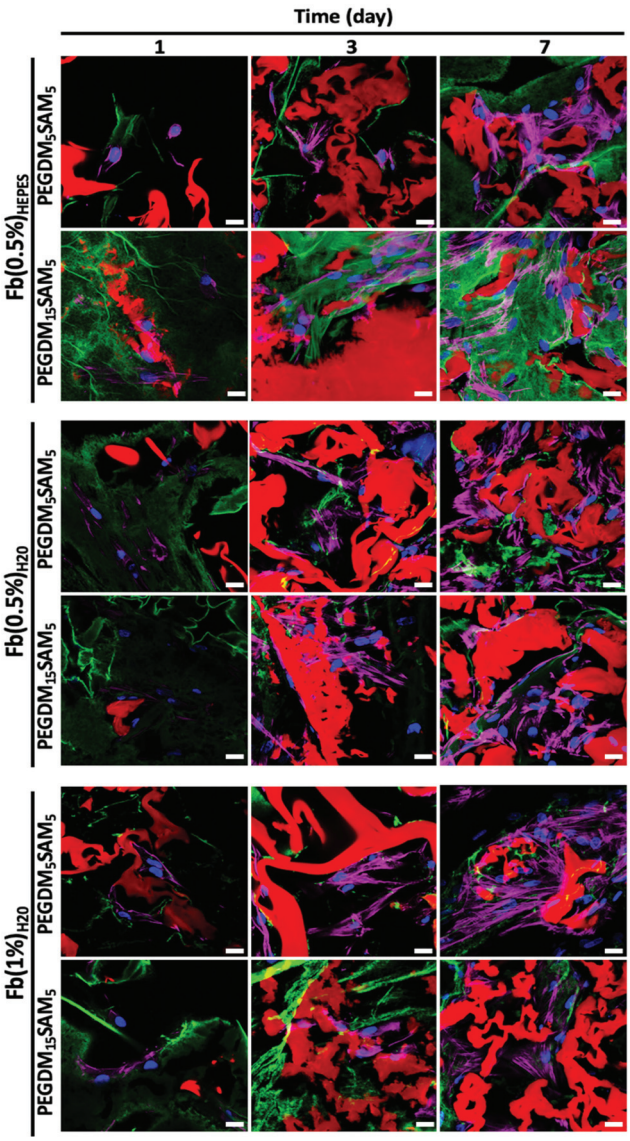

Fig. 6 Cell morphology of HDFs in fibrin/PEGDM-*co*-SAM sequential IPN hydrogels. HDFs were cultured in various fibrin/PEGDM-*co*-SAM IPN constructs: fibrin/$PEGDM_5SAM_5$ and fibrin/$PEGDM_{15}SAM_5$ fabricated with different fibrin formulations: $Fb(0.5\%)_{HEPES}$, $Fb(0.5\%)_{H_2O}$ or $Fb(1\%)_{H_2O}$. Cell morphology was analyzed by confocal microscopy after 1, 3, and 7 d of culture depicting F-actin (dark pink), nuclei (blue), fibrin (green) and PEGDM-*co*-SAM (red). Scale bar = 20 μm.

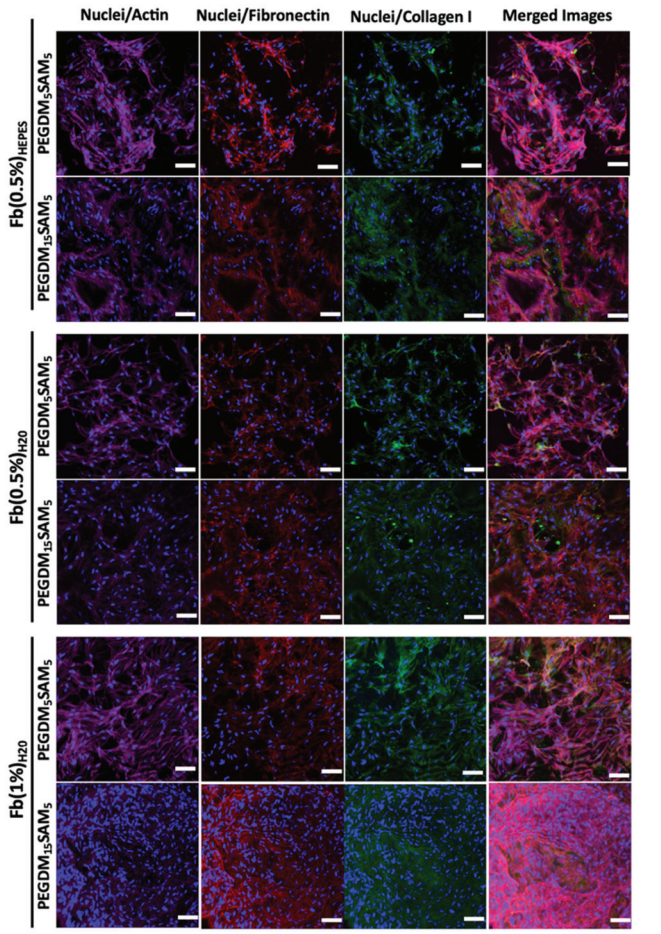

Fig. 7 Evaluation of HDF-derived extracellular matrix deposition on fibrin/PEGDM-*co*-SAM sequential IPN hydrogels. Secretion of two endogenous extracellular matrix proteins (collagen I and fibronectin) from HFD after 1-week culture in various IPN constructs: fibrin/$PEGDM_5SAM_5$ and fibrin/$PEGDM_{15}SAM_5$ fabricated with different fibrin formulations: Fb(0.5%)HEPES, $Fb(0.5\%)_{H_2O}$ or $Fb(1\%)_{H_2O}$. Samples were stained and analyzed by confocal microscopy: F-actin (dark pink), nuclei (blue), fibronectin (red), and collagen I (green). Scale bar = 100 μm.

across all the biomaterials investigated with no significant difference between them.

Collectively, this set of data suggests that our IPNs form suitable environments for cell infiltration and remodeling.

***In vivo* studies.** Lastly, we tested the biomaterials in an animal model. We assessed the biocompatibility, the biointegration and the biodegradation of fibrin/PEGDM-*co*-SAM IPN hydrogels in nude mice (Fig. 8). Fibrin/$PEGDM_5SAM_5$ and fibrin/$PEGDM_{15}SAM_5$ hydrogels made with $Fb(0.5\%)_{HEPES}$ were implanted in mice due to their superior mechanical properties. Commercially available porcine collagen acellular dermis, which is currently used for skin wound healing and soft tissue augmentation, was also implanted as the control group. Within the first week following implantation, mice showed signs of scar-free healing with complete absorption of surgical sutures. Furthermore, the animals did not display any apparent signs of erythema, edema or necrosis at the surgical sites. At week 4, the histological analysis on the explanted samples displayed no major immunological responses across the two types of biomaterials tested. We observed minimal to moderate resorptive macrophagic responses (presence of epithelioid macrophages as well as few multinucleated giant cells in contact with both implants) and thin fibrous capsules around the materials. The formation of thin fibrous capsules surrounding the implants is a physiological response to a foreign body following implantation.[15,71–74] The mild host immune reaction after biomaterial implantation could also be related to the immunogenicity of bovine SA. To address this challenge, albumin from mouse serum could be used in the IPN gel formulation to further enhance their biocompatibility.

Additionally, even though SA was incorporated as an enzymatically degradable entity, the biomaterials seemed to remain intact up to 1 month following implantation, suggesting slow biodegradation. This could be attributed to the presence of poly(methyl methacrylate) segments within the polymer network, which are known to poorly degradable *in vivo*.[15,75] Various strategies could be investigated to make these IPN constructs more prone to biodegradation.[76] One strategy could be to use biodegradable PEG-based block copolymers (*e.g.*, PEG-*co*-polyglycolic acid) which contain hydrolysable ester bonds.[43,77] Lastly, signs of tissue remodeling were observed with host fibroblasts, *de novo* synthesis of collagen and early stages of angiogenesis (*i.e.*, neovascularization) within the explanted constructs, indicating good biointegration.[14] Therefore, these constructs have great potential for dermal tissue regeneration and wound healing applications.[4,5,41,78] However, follow-up validation studies with relevant wound healing models are recommended.

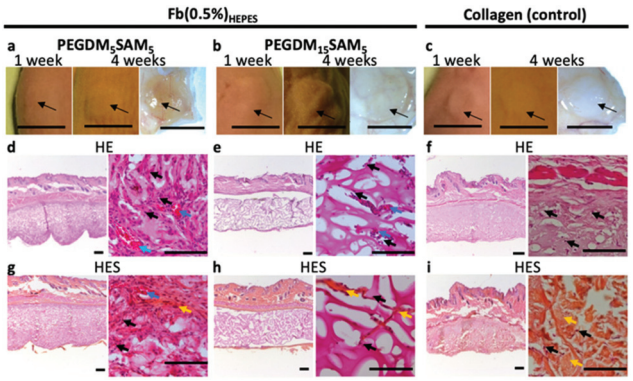

Fig. 8 Histological analysis of subcutaneously implanted PEGDM-*co*-SAM sequential IPN hydrogels. Explanted (a) $PEGDM_5SAM_5$ and (b) $PEGDM_{15}SAM_5$ sequential IPN hydrogels made with $Fb(0.5\%)_{HEPES}$ following 1 week (left image) and 4 weeks (center image) implantation in mice. (c) Commercially available collagen matrices were implanted as controls. Black arrows show the implants. (d–f) H&E and (g–i) H&ES staining of (d and g) $PEGDM_5SAM_5$ and (e and h) $PEGDM_{15}SAM_5$ sequential IPN hydrogels made with $Fb(0.5\%)_{HEPES}$ 1 month post-subcutaneous implantations. (f and i) Commercially available collagen matrices were implanted as controls. Staining highlights the macroporous polymeric network of IPN hydrogels (interconnected dark purple network), infiltrated cells (indicated with black arrows), blood vessels (indicated with blue arrows) and collagen deposition (indicated with orange arrows). (d–i, left) Histological images show zoomed out and (d–i, right) zoomed in views. Scale bars: (a–c, left and middle) 1 cm, (a–c, right) 5 mm, (d–i, left) 500 μm, (d–i, right) 50 μm.

Conclusions

In this study, we report on an innovative synthetic approach to engineer macroporous and interconnected fibrin-based sequential IPN hydrogels for dermal tissue engineering. The engineered IPN hydrogels combined both the superior mechanical properties of PEG and the intrinsic biological features of fibrin. In addition, properties of IPNs can be fine-tuned based on the precursor concentration and solution used during the fabrication process. Their unique macroporous network and biological properties enhanced dermal fibroblast adhesion, infiltration, and proliferation *in vitro*. Additionally, these IPN hydrogels are biocompatible as demonstrated by a minimal host inflammatory response when implanted subcutaneously in mice. Furthermore, they promoted local tissue remodeling as indicated with host cellular infiltration, *de novo* ECM synthesis, and neovascularization. Altogether, our data suggest that these macroporous fibrin-based sequential IPN hydrogels have great potential for dermal tissue engineering and other relevant biomedical applications.

Conflicts of interest

The authors declare that there is no conflict of interest regarding the publication of this article.

Acknowledgements

This work was supported by the ANR TECSAN Fibriderm (project number ANR-13-TECS-0014) and the Picardy region. Sidi A. Bencherif acknowledges financial support from an NSF CAREER award (DMR 1847843). We wish to thank Fréderic

Nadaud for his assistance with the SEM and ESEM characterizations. We also thank Elisabeth Van Hecke for her help with the rheology measurements, Elise Prost for her technical assistance with the NMR measurements, and Ulysse Peirera for his helpful discussions.

Notes and references

1 R. V. Shevchenko, M. Eeman, B. Rowshanravan, I. U. Allan, I. N. Savina, M. Illsley, M. Salmon, S. L. James, S. V. Mikhalovsky and S. E. James, *Acta Biomater.*, 2014, **10**, 3156–3166.
2 H. Debels, M. Hamdi, K. Abberton and W. Morrison, *Plast. Reconstr. Surg. Glob. Open*, 2015, **3**, e284.
3 L. Ma, C. Gao, Z. Mao, J. Zhou, J. Shen, X. Hu and C. Han, *Biomaterials*, 2003, **24**, 4833–4841.
4 A. Francesko, P. Petkova and T. Tzanov, *Curr. Med. Chem.*, 2018, **25**, 5782–5797.
5 H. Sorg, D. J. Tilkorn, S. Hager, J. Hauser and U. Mirastschijski, *Eur. Surg. Res.*, 2017, **58**, 81–94.
6 S. P. Zhong, Y. Z. Zhang and C. T. Lim, *Wiley Interdiscip. Rev.: Nanomed. Nanobiotechnol.*, 2010, **2**, 510–525.
7 K. W. Ng, H. L. Khor and D. W. Hutmacher, *Biomaterials*, 2004, **25**, 2807–2818.
8 J. Rnjak, Z. Li, P. K. M. Maitz, S. G. Wise and A. S. Weiss, *Biomaterials*, 2009, **30**, 6469–6477.
9 J. Rnjak-Kovacina, S. G. Wise, Z. Li, P. K. M. Maitz, C. J. Young, Y. Wang and A. S. Weiss, *Biomaterials*, 2011, **32**, 6729–6736.
10 C. Gao, D. Wang and J. Shen, *Polym. Adv. Technol.*, 2003, **14**, 373–379.
11 B. K. Boekema, M. Vlig, L. O. Damink, E. Middelkoop, L. Eummelen, A. V. Bühren and M. M. W. Ulrich, *J. Mater. Sci. Mater. Med.*, 2014, **25**, 423–433.
12 Z. Zhu, Y.-M. Wang, J. Yang and X.-S. Luo, *Plast. Aesthetic Res.*, 2017, **4**, 219–227.
13 H.-M. Wang, Y.-T. Chou, Z.-H. Wen, Z.-R. Wang, C.-H. Chen and M.-L. Ho, *PLoS One*, 2013, **8**, e56330.
14 O. Gsib, C. Egles and S. A. Bencherif, *J. Mol. Biol. Biotechnol.*, 2017, **2**, 1.
15 O. Gsib, J.-L. Duval, M. Goczkowski, M. Deneufchatel, O. Fichet, V. Larreta-Garde, S. A. Bencherif and C. Egles, *Nanomaterials*, 2017, **7**, 436.
16 O. Gsib, M. Deneufchatel, M. Goczkowski, M. Trouillas, M. Resche-Guigon, S. Bencherif, O. Fichet, J.-J. Lataillade, V. Larreta-Garde and C. Egles, *IRBM*, 2018, **39**, 103–108.
17 T. V. Anilkumar, J. Muhamed, A. Jose, A. Jyothi, P. V. Mohanan and L. K. Krishnan, *Biologicals*, 2011, **39**, 81–88.
18 W. D. Spotnitz, *World J. Surg.*, 2010, **34**, 632–634.
19 P. A. Janmey, J. P. Winer and J. W. Weisel, *J. R. Soc., Interface*, 2009, **6**, 1–10.
20 A. L. Mazlyzam, B. S. Aminuddin, N. H. Fuzina, M. M. Norhayati, O. Fauziah, M. R. Isa, L. Saim and B. H. I. Ruszymah, *Burns*, 2007, **33**, 355–363.
21 A. Meana, J. Iglesias, M. Del Rio, F. Larcher, B. Madrigal, M. F. Fresno, C. Martin, F. San Roman and F. Tevar, *Burns*, 1998, **24**, 621–630.
22 T. Sun, J. Haycock and S. Macneil, *Biomaterials*, 2006, **27**, 3459–3465.
23 Z. J. Rogers, M. P. Zeevi, R. Koppes and S. A. Bencherif, *Bioelectricity*, 2020, **2**, 279–292.
24 N. Nakagawa, M. Matsumoto and S. Sakai, *Skin Res. Technol.*, 2010, **16**, 137–141.
25 P. Matricardi, C. Di Meo, T. Coviello, W. E. Hennink and F. Alhaique, *Adv. Drug Delivery Rev.*, 2013, **65**, 1172–1187.
26 E. Akpalo, L. Bidault, M. Boissière, C. Vancaeyzeele, O. Fichet and V. Larreta-Garde, *Acta Biomater.*, 2011, **7**, 2418–2427.
27 M. W. Tibbitt and K. S. Anseth, *Biotechnol. Bioeng.*, 2009, **103**, 655–663.
28 L. Bidault, M. Deneufchatel, C. Vancaeyzeele, O. Fichet and V. Larreta-Garde, *Biomacromolecules*, 2013, **14**, 3870–3879.
29 O. M. Benavides, J. P. Quinn, S. Pok, J. Petsche Connell, R. Ruano and J. G. Jacot, *Tissue Eng., Part A*, 2015, **21**, 1185–1194.
30 F. Lee and M. Kurisawa, *Acta Biomater.*, 2013, **9**, 5143–5152.
31 P. Losi, E. Briganti, A. Magera, D. Spiller, C. Ristori, B. Battolla, M. Balderi, S. Kull, A. Balbarini, R. Di Stefano and G. Soldani, *Biomaterials*, 2010, **31**, 5336–5344.
32 Y. Zhang, P. Heher, J. Hilborn, H. Redl and D. A. Ossipov, *Acta Biomater.*, 2016, **38**, 23–32.
33 E. S. Dragan, *Chem. Eng. J.*, 2014, **243**, 572–590.
34 D. Myung, D. Waters, M. Wiseman, P.-E. Duhamel, J. Noolandi, C. N. Ta and C. W. Frank, *Polym. Adv. Technol.*, 2008, **19**, 647–657.
35 A. Lohani, G. Singh, S. S. Bhattacharya and A. Verma, *J. Drug Delivery*, 2014, **2014**, 583612.
36 A. Shikanov, M. Xu, T. K. Woodruff and L. D. Shea, *Biomaterials*, 2009, **30**, 5476–5485.
37 S. L. Rowe and J. P. Stegemann, *Biomacromolecules*, 2006, **7**, 2942–2948.
38 L. Bidault, M. Deneufchatel, M. Hindié, C. Vancaeyzeele, O. Fichet and V. Larreta-Garde, *Polymer*, 2015, **62**, 19–27.
39 G. Chen, T. Ushida and T. Tateishi, *Macromol. Biosci.*, 2002, **2**, 67–77.
40 T. M. Freyman, I. V. Yannas and L. J. Gibson, *Prog. Mater. Sci.*, 2001, **46**, 273–282.
41 A. Amirsadeghi, A. Jafari, L. J. Eggermont, S.-S. Hashemi, S. A. Bencherif and M. Khorram, *Biomater. Sci.*, 2020, **8**, 4073–4094.
42 N. Annabi, J. W. Nichol, X. Zhong, C. Ji, S. Koshy, A. Khademhosseini and F. Dehghani, *Tissue Eng., Part B*, 2010, **16**, 371–383.
43 S. A. Bencherif, T. M. Braschler and P. Renaud, *J. Periodontal Implant Sci.*, 2013, **43**, 251–261.
44 S. A. Bencherif, J. A. Sheehan, J. O. Hollinger, L. M. Walker, K. Matyjaszewski and N. R. Washburn, *J. Biomed. Mater. Res., Part A*, 2009, **90**, 142–153.
45 S. Lin-Gibson, S. Bencherif, J. M. Antonucci, R. L. Jones and F. Horkay, *Macromol. Symp.*, 2005, **227**, 243–254.

46 P. Villard, M. Rezaeeyazdi, T. Colombani, K. Joshi-Navare, D. Rana, A. Memic and S. A. Bencherif, *Adv. Healthcare Mater.*, 2019, **8**, 1900679.
47 A. Memic, M. Rezaeeyazdi, P. Villard, Z. J. Rogers, T. Abudula, T. Colombani and S. A. Bencherif, *Macromol. Mater. Eng.*, 2020, **305**, 1900824.
48 Z. J. Rogers and S. A. Bencherif, *Gels*, 2019, **5**, 46.
49 L. J. Eggermont, Z. J. Rogers, T. Colombani, A. Memic and S. A. Bencherif, *Trends Biotechnol.*, 2020, **38**, 418–431.
50 A. Memic, T. Colombani, L. J. Eggermont, M. Rezaeeyazdi, J. Steingold, Z. J. Rogers, K. J. Navare, H. S. Mohammed and S. A. Bencherif, *Adv. Ther.*, 2019, **2**, 1800114.
51 K. Joshi-Navare, L. J. Eggermont, Z. J. Rogers, H. S. Mohammed, T. Colombani and S. A. Bencherif, in *Racing for the Surface: Pathogenesis of Implant Infection and Advanced Antimicrobial Strategies*, ed. B. Li, T. F. Moriarty, T. Webster and M. Xing, Springer International Publishing, Cham, 2020, pp. 511–542.
52 J. Kim, S. A. Bencherif, W. A. Li and D. J. Mooney, *Macromol. Rapid Commun.*, 2014, **35**, 1578–1586.
53 S. Kennedy, S. Bencherif, D. Norton, L. Weinstock, M. Mehta and D. Mooney, *Adv. Healthcare Mater.*, 2014, **3**, 500–507.
54 M.-E. Han, S.-H. Kim, H. D. Kim, H.-G. Yim, S. A. Bencherif, T.-I. Kim and N. S. Hwang, *Int. J. Biol. Macromol.*, 2016, **93**, 1410–1419.
55 M. Rezaeeyazdi, T. Colombani, A. Memic and S. A. Bencherif, *Materials*, 2018, **11**, 1374.
56 B. Dhandayuthapani, Y. Yoshida, T. Maekawa and D. S. Kumar, *Int. J. Polym. Sci.*, 2011, **2011**, 290602.
57 V. Sharma, N. Patel, N. Kohli, N. Ravindran, L. Hook, C. Mason and E. García-Gareta, *Biomed. Mater.*, 2016, **11**, 055001.
58 C. Faure and G. Barry, *Monit. Hosp.*, 2011, **240**, 33–44.
59 C. S. L. Müller, C. Schiekofer, R. Körner, C. Pföhler and T. Vogt, *J. Dtsch. Dermatol. Ges.*, 2013, **11**, 537–548.
60 O. Okay, in *Hydrogel Sensors and Actuators*, Springer, Berlin, Heidelberg, 2009, pp. 1–14.
61 S. MacNeil, *Mater. Today*, 2008, **11**, 26–35.
62 V. Abbate, X. Kong and S. S. Bansal, *Enzyme Microb. Technol.*, 2012, **50**, 130–136.
63 J. M. Zuidema, C. J. Rivet, R. J. Gilbert and F. A. Morrison, *J. Biomed. Mater. Res., Part B*, 2014, **102**, 1063–1073.
64 N. A. Kurniawan, T. H. S. van Kempen, S. Sonneveld, T. T. Rosalina, B. E. Vos, K. A. Jansen, G. W. M. Peters, F. N. van de Vosse and G. H. Koenderink, *Langmuir*, 2017, **33**, 6342–6352.
65 H. E. Davis, S. L. Miller, E. M. Case and J. K. Leach, *Acta Biomater.*, 2011, **7**, 691–699.
66 N. Laurens, P. Koolwijk and M. P. M. De Maat, *J. Thromb. Haemostasis*, 2006, **4**, 932–939.
67 H. Phillips, *Nat. News*, 1998.
68 B. Holt, A. Tripathi and J. Morgan, *J. Biomech.*, 2008, **41**, 2689–2695.
69 K. Wolf, S. Alexander, V. Schacht, L. M. Coussens, U. H. von Andrian, J. van Rheenen, E. Deryugina and P. Friedl, *Semin. Cell Dev. Biol.*, 2009, **20**, 931–941.
70 S. Stenman and A. Vaheri, *J. Exp. Med.*, 1978, **147**, 1054–1064.
71 R. Shah, M. C. Pierce and F. H. Silver, *J. Biomed. Mater. Res., Part A*, 2017, **105**, 15–22.
72 D. Wolfram, B. Oberreiter, C. Mayerl, E. Soelder, H. Ulmer, H. Piza-Katzer, G. Wick and A. Backovic, *Immunol. Lett.*, 2008, **118**, 96–100.
73 D.-J. Li, K. Ohsaki, K. Ii, P.-C. Cui, Q. Ye, K. Baba, Q.-C. Wang, S. Tenshin and T. Takano-Yamamoto, *J. Biomed. Mater. Res.*, 1999, **45**, 322–326.
74 D. Bakker, C. A. van Blitterswijk, S. C. Hesseling, J. J. Grote and W. T. Daems, *Biomaterials*, 1988, **9**, 14–23.
75 R. G. Hill, in *Biomaterials, Artificial Organs and Tissue Engineering*, ed. L. L. Hench and J. R. Jones, Woodhead Publishing, 2005, pp. 37–47.
76 S. Lin-Gibson, S. Bencherif, J. A. Cooper, S. J. Wetzel, J. M. Antonucci, B. M. Vogel, F. Horkay and N. R. Washburn, *Biomacromolecules*, 2004, **5**, 1280–1287.
77 S. A. Bencherif, A. Srinivasan, J. A. Sheehan, L. M. Walker, C. Gayathri, R. Gil, J. O. Hollinger, K. Matyjaszewski and N. R. Washburn, *Acta Biomater.*, 2009, **5**, 1872–1883.
78 A. Grada, J. Mervis and V. Falanga, *J. Invest. Dermatol.*, 2018, **138**, 2095–2105.

